

Dissecting components of the *Campylobacter jejuni* *fetMP-fetABCDEF* gene cluster under iron limitation

Tomas Richardson-Sanchez,¹ Anson C. K. Chan,¹ Brendil Sabatino,¹ Helen Lin,¹ Erin C. Gaynor,¹ Michael E. P. Murphy¹

AUTHOR AFFILIATION See affiliation list on p. 13.

ABSTRACT *Campylobacter jejuni* is a leading cause of bacterial gastroenteritis worldwide. Acute infection can be an antecedent to highly debilitating long-term sequelae. The expression of iron acquisition systems is vital for *C. jejuni* to survive the low iron availability within the human gut. The *C. jejuni* *fetMP-fetABCDEF* gene cluster is known to be upregulated during human infection and under iron limitation. While FetM and FetP have been functionally linked to iron transport in prior work, here we assess the contribution of each of the downstream genes (*fetABCDEF*) to *C. jejuni* growth during both iron-depleted and iron-replete conditions. Significant growth impairment was observed upon disruption of *fetA*, *fetB*, *fetC*, and *fetD*, suggesting a role in FetMP-mediated iron acquisition for each encoded protein. FetA expression was not dependent on the presence of FetB, FetC, FetD, FetE, or FetF. The functions of the putative thioredoxins FetE and FetF were redundant under iron-limited growth, requiring a double deletion (Δ *fetEF*) to exhibit a growth defect. *C. jejuni* FetE was expressed, and the structure was solved to 1.50 Å, revealing structural similarity to thiol-disulfide oxidases. Functional characterization in biochemical assays showed that FetE reduced insulin at a slower rate than *Escherichia coli* Trx and that together, FetEF promoted substrate oxidation in cell extracts, suggesting that FetE (and presumably FetF) are oxidoreductases that can mediate oxidation *in vivo*. This study advances our understanding of the contributions of the *fetMP-fetABCDEF* gene cluster to virulence at a genetic and functional level, providing foundational knowledge toward mitigating *C. jejuni*-related morbidity and mortality.

IMPORTANCE *Campylobacter jejuni* is a bacterium that is prevalent in the ceca of farmed poultry such as chickens. Consumption of ill-prepared poultry is thus the most common route by which *C. jejuni* infects the human gut to cause a typically self-limiting but severe gastrointestinal illness that can be fatal to very young, old, or immunocompromised people. The lack of a vaccine and an increasing resistance to current antibiotics highlight a need to better understand the mechanisms that make *C. jejuni* a successful human pathogen. This study focused on the functional components of one such mechanism—a molecular system that helps *C. jejuni* thrive despite the restriction on growth-available iron by the human body, which typically defends against pathogens. In providing a deeper understanding of how this system functions, this study contributes toward the goal of reducing the enormous global socioeconomic burden caused by *C. jejuni*.

KEYWORDS *Campylobacter jejuni*, iron transport, Fet system genes, thiol-disulfide oxidoreductase, X-ray crystallography

Campylobacter jejuni is a Gram-negative ϵ -proteobacterium and a leading cause of bacterial diarrheal disease worldwide. *C. jejuni* is a commensal in the intestinal mucosa of many wild and domesticated animals, commonly colonizing farmed poultry flocks and then undergoing zoonotic transmission to humans, by, for example, the consumption of undercooked poultry or cross-contamination of other food with raw

Editor Carlos J. Blondel, Universidad Andres Bello, Santiago, Chile

Address correspondence to Michael E. P. Murphy, michael.murphy@ubc.ca.

Tomas Richardson-Sanchez and Anson C. K. Chan contributed equally to this article. Author order was determined by greater contribution to experimental design.

Erin C. Gaynor and Michael E. P. Murphy were co-supervisors of this work. These authors contributed equally to project oversight and are listed in alphabetical order.

The authors declare no conflict of interest.

See the funding table on p. 13.

Dr. Erin Gaynor, a Professor in the Department of Microbiology and Immunology, has been a valued member of the The University of British Columbia community for the last 20 years since her recruitment as an Assistant Professor in June 2003. Sadly, she passed away in her home on Monday, March 6, 2023. Erin is remembered for her wit and creative drive to excel as a teacher and microbiologist, and her kind and caring heart. She will be deeply missed.

Received 4 October 2023

Accepted 14 November 2023

Published 14 December 2023

Copyright © 2023 Richardson-Sanchez et al. This is an open-access article distributed under the terms of the [Creative Commons Attribution 4.0 International license](https://creativecommons.org/licenses/by/4.0/).

poultry juice (1, 2). Acute human infection results in severe watery to bloody diarrhea and can also be an antecedent to highly debilitating long-term sequelae, such as inflammatory bowel diseases and autoimmune disorders (3–5). The high socioeconomic burden and impact on human health have been made worse by the inability to produce an effective vaccine and the increasing levels of antibiotic resistance in isolates from both hospitals (6, 7) and poultry meat (8).

Successful *C. jejuni* colonization of the human intestinal mucosa is dependent on a range of factors, including the expression of systems to acquire essential micronutrients such as iron. Recent transcriptional studies on *C. jejuni* have demonstrated the upregulation of an eight gene cluster (*CJJ81176_1649–1656*, hereinafter named *fetMP-fetABCDEF*), during human infection (9). Also, our group has shown increased expression of *fetMP-fetABCDE* upon exposure to human fecal metabolites (10), indicating a likely role in pathogenesis. The two upstream genes, *fetM* (*CJJ81176_1649*) and *fetP* (*CJJ81176_1650*, also known as *p19*), encode the FetMP iron transport system, which has been shown to be important for growth under iron-limited conditions (11, 12). The six downstream genes *fetABCDEF* (*CJJ81176_1651–1656*) have not previously been characterized individually, but collectively have been shown to be strongly upregulated alongside *fetMP* during iron restriction and upon deletion of *fur*, which encodes the ferric uptake regulator protein (13–15). Two other studies have observed *C. jejuni* growth defects under iron restriction upon disruption of the *fetMP-fetABCDEF* gene cluster, either by deletion of *fetP* (11) or, as our groups recently demonstrated, simultaneous deletion of all six downstream genes (Δ *fetABCDEF*) (10), with growth defects restored upon iron supplementation or complementation with the wild-type (WT) gene cluster. Additionally, *C. jejuni* exhibits a biphasic phenotype to the antibiotic streptomycin. Rather than a unimodal concentration-dependent inhibitory effect, wild-type *C. jejuni* exhibits streptomycin tolerance at moderate antibiotic concentrations. This tolerance is lost upon the deletion of *fetABCDEF* but can be restored by supplementing the deletion strain with iron, supporting the role of this cluster in iron metabolism. *C. jejuni* Δ *fetABCDEF* also has increased acid sensitivity and higher resistance to oxidative stress (10). These transcriptional and phenotypic studies link *fetABCDEF* to a role in *C. jejuni* pathogenesis, providing greater impetus to investigate each individual component of the *fetMP-fetABCDEF* gene cluster.

Gene clusters homologous to *fetMP-fetABCDEF* have been identified in 33 diverse bacterial species across six phyla, including 21 species that are associated with human disease (10). The *C. jejuni* *fetMP-fetABCDEF* gene cluster spans a genomic region of 8.1 kb and consists of two upstream genes (*fetMP*) separated from six downstream genes (*fetABCDEF*) by an 82 base intergenic region (Fig. 1A). Upstream of the *fetM* start codon is a Fur binding sequence (10 bases upstream) and a putative primary transcription start site (54 bases upstream) (16), suggesting *fetMP-fetABCDEF* may be transcribed as one operon.

In silico domain analysis of the proteins encoded by *fetMP-fetABCDEF* (Fig. 1B) allows the identification of putative functions in cases where functional studies on the proteins or their homologs are lacking. FetM is yet to be characterized in *C. jejuni*, although the *Escherichia coli* homolog has been demonstrated to be an iron transporter of the “oxidase-dependent iron transporter” family (17, 18). FetP has been characterized as a periplasmic iron binding protein in *C. jejuni* (11), as well as in *E. coli* (18), *Bordetella* (19), and *Yersinia pestis* (20). The FetMP iron uptake system was suggested to import ferric-rhodotorulic acid (A. Stintzi and J. M. Ketley, unpublished data) (21), but studies have demonstrated that *C. jejuni* cannot utilize this siderophore for growth (22, 23).

No prior functional studies have been reported for FetABCDEF or their homologs. We predict that these six gene products include a putative membrane protein (encoded by *fetA*), a putative ATP-binding cassette (ABC) transporter (encoded by *fetBCD*), and two putative thioredoxins (encoded by *fetEF*). FetA is predicted to contain eight transmembrane domains, a domain of unknown function (DUF2318), and a YHS domain. The genes *fetB* and *fetC* encode domains consistent with ABC transporter permeases, and *fetD*

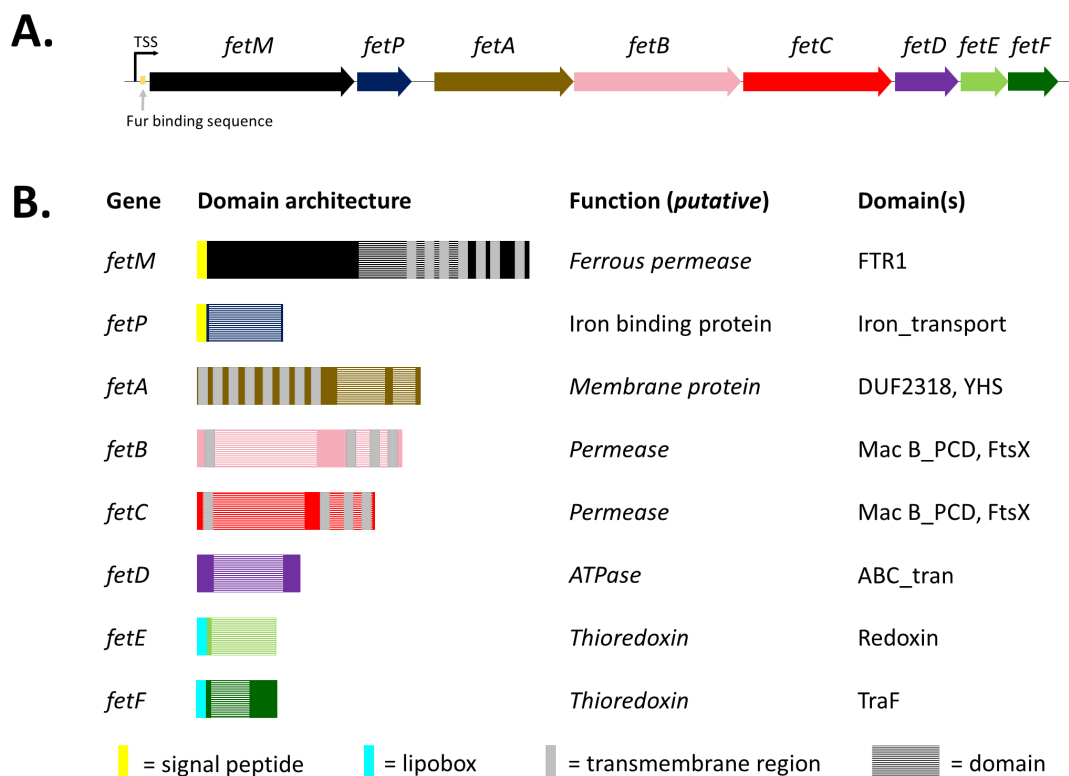


FIG 1 Putative operonic structure, domain architecture, and model with predicted functions of the *fetMP-fetABCDEF* gene cluster. (A) Proposed operon structure in *C. jejuni* wild-type strain 81–176 with primary transcription start site (TSS) and Fur binding sequence. (B) Gene function and domain architecture. Signal peptides and protein lipitation sites (lipoboxes) predicted by SignalP-5.0, transmembrane helices by TMHMM Server v2.0, and domain predictions by Pfam 32.0.

encodes conserved sequence motifs that are vital for ATP binding and hydrolysis. Thus, *fetBCD* is predicted to encode an ABC transporter for active transport of substrates across the inner membrane. Overall, the *fetMP-fetABCDEF* gene cluster is predicted to encode four distinct inner membrane proteins, which would be unusual for an iron uptake system. The genes *fetE* and *fetF* are predicted to encode single-domain, membrane-associated thioredoxin oxidoreductases. Oxidoreductases can mediate transitions between Cys-Cys disulfide and dithiol groups within proteins, a function dependent on a conserved active site motif (CXXC) (24) that is present in the FetE (CPSC) and FetF (CGVC) protein sequences.

To ascribe the phenotypes observed for Δ *fetABCDEF* (10) to specific genes within the cluster and to provide insight into the essentiality of each functional unit for iron acquisition, this study used a genetic approach to test individual *fet* gene deletion strains for sensitivity to iron availability and to the antibiotic streptomycin. Comparable degrees of growth impairment were observed under low iron upon disruption of *fetM*, *fetP*, *fetA*, *fetB*, *fetC*, and *fetD*. Based on single and double-mutant analyses, we predict that *fetE* and *fetF* encode gene products that function redundantly under iron limitation. All *fet* deletion strains exhibited an increased sensitivity to streptomycin, implicating iron homeostasis as a determinant of growth modality and resistance during streptomycin exposure. Structural biology and biochemical assays allowed further investigation into the function of FetE as a thiol-disulfide oxidoreductase that may act as an oxidase *in vivo*.

RESULTS

Sensitivity to iron availability for *C. jejuni* strains

To investigate the contribution of the *fetMP-fetABCDEF* gene cluster components toward growth under different levels of iron availability, gene deletion (Δ) and complemented

(^c) *C. jejuni* strains were constructed for *fetM*, *fetA*, *fetB*, *fetC*, *fetD*, *fetE*, and *fetF* (Fig. S1). To account for the potential redundancy of the putative thioredoxins FetE and FetF, a double deletion ($\Delta fetEF$) and corresponding complemented (*fetEF^c*) strain were also constructed. Wild-type *C. jejuni* 81–176 was used as a control, and *C. jejuni* strains corresponding to *fetP* ($\Delta fetP$ and *fetP^c*) and the six gene *fet* cluster ($\Delta fetABCDEF$ and *fetABCDEF^c*) were used as standards in growth curve experiments (10, 11).

All *C. jejuni* strains were cultured in iron-restricted Mueller-Hinton (MH) broth, standard MH broth, and iron-supplemented MH broth (Fig. 2 and 3). Iron restriction was achieved by supplementing MH broth with the high-affinity ferric iron chelator desferrioxamine B (DFO), a siderophore that cannot be used by *C. jejuni* as an iron source. Iron supplementation was achieved by supplementing MH broth with 100 μ M ferric chloride. As the iron content in MH medium varies between brands and product batches (25), all growth experiments used a single batch of MH medium, and the DFO concentration was optimized to 5 μ M from a test range of 0–20 μ M (data not shown). The total Fe content of the standard growth medium was measured at 7 μ M by inductively coupled plasma mass spectrometry (ICP-MS). The growth of *C. jejuni* strains under different levels of iron availability was monitored by OD₆₀₀ (Fig. 2A) and colony forming units (CFU, Fig. 3). The sensitivity of individual strains to changes in iron availability was assessed by comparing cell densities (OD₆₀₀) after 30 h of growth under each condition (Fig. 2B).

Growth defects demonstrated by gene deletion mutants were fully restored to that of wildtype by ectopic chromosomal complementation. Overall, the trends in growth observed by OD₆₀₀ (Fig. 2) were consistent with those observed by CFU (Fig. 3), with complementation diminishing the possibility that these phenotypes resulted from polar effects on downstream genes. The phenotypic trends under iron limitation observed for the *C. jejuni* strains that were being used as experimental standards ($\Delta fetABCDEF$, *fetABCDEF^c*, $\Delta fetP$, and *fetP^c*) were also consistent with those in the original studies (10, 11).

Gene deletion strains $\Delta fetM$, $\Delta fetP$, $\Delta fetA$, $\Delta fetB$, $\Delta fetC$, $\Delta fetD$, and $\Delta fetABCDEF$ exhibited significant growth defects compared to wildtype by OD₆₀₀ at 24 and 30 h under all levels of iron availability. Additionally, growth after 30 h for $\Delta fetP$, $\Delta fetA$, $\Delta fetB$, $\Delta fetC$, $\Delta fetD$, and $\Delta fetABCDEF$ strongly correlated with the level of iron availability for each strain. The growth of $\Delta fetM$ varied little upon iron restriction or supplementation, indicating insensitivity to iron availability (Fig. 2B). These trends for growth defects and sensitivity to iron availability for $\Delta fetM$, $\Delta fetP$, $\Delta fetA$, $\Delta fetB$, $\Delta fetC$, $\Delta fetD$, and $\Delta fetABCDEF$ were consistent with CFU data (Fig. 3).

By both OD₆₀₀ and CFU, individual $\Delta fetE$ and $\Delta fetF$ strains did not demonstrate growth defects and were similarly insensitive to iron availability when compared to wildtype. The double deletion mutant $\Delta fetEF$, however, had significantly reduced growth by OD₆₀₀ and CFU/mL compared to wildtype, $\Delta fetE$, and $\Delta fetF$ under all levels of iron availability and exhibited sensitivity to iron levels.

Streptomycin sensitivity of *C. jejuni* strains

Deletion of the *fetABCDEF* gene cluster was shown to disrupt streptomycin resistance of *C. jejuni*, which was restored with iron supplementation (10). To investigate the role of each gene in biphasic streptomycin resistance, all deletion strains were assayed for minimum inhibitory concentration (MIC) of streptomycin (Fig. S2). Control wild-type *C. jejuni* cultures exhibited streptomycin-sensitive growth from 0 to 1 μ g/mL of streptomycin and streptomycin-tolerant growth from 1 to 4 μ g/mL of streptomycin.

All *C. jejuni* gene deletion strains demonstrated increased sensitivity to streptomycin. $\Delta fetM$, $\Delta fetA$, $\Delta fetB$, $\Delta fetC$, $\Delta fetD$, $\Delta fetABCDEF$, and $\Delta fetP$ exhibited unimodal growth and hence a loss of biphasic phenotype (Fig. S2A). At 1 μ g/mL of streptomycin, $\Delta fetM$, $\Delta fetA$, and $\Delta fetD$ demonstrated minimal growth similar to $\Delta fetABCDEF$, $\Delta fetB$ and $\Delta fetP$ demonstrated an intermediate phenotype, and $\Delta fetC$ was similar to wildtype. Increasing the concentration to 2 and 4 μ g/mL of streptomycin, $\Delta fetM$, $\Delta fetP$, $\Delta fetA$, $\Delta fetB$, $\Delta fetC$, and $\Delta fetD$ all showed similar growth to $\Delta fetABCDEF$ (Fig. S2A), whereas $\Delta fetE$, $\Delta fetF$, and

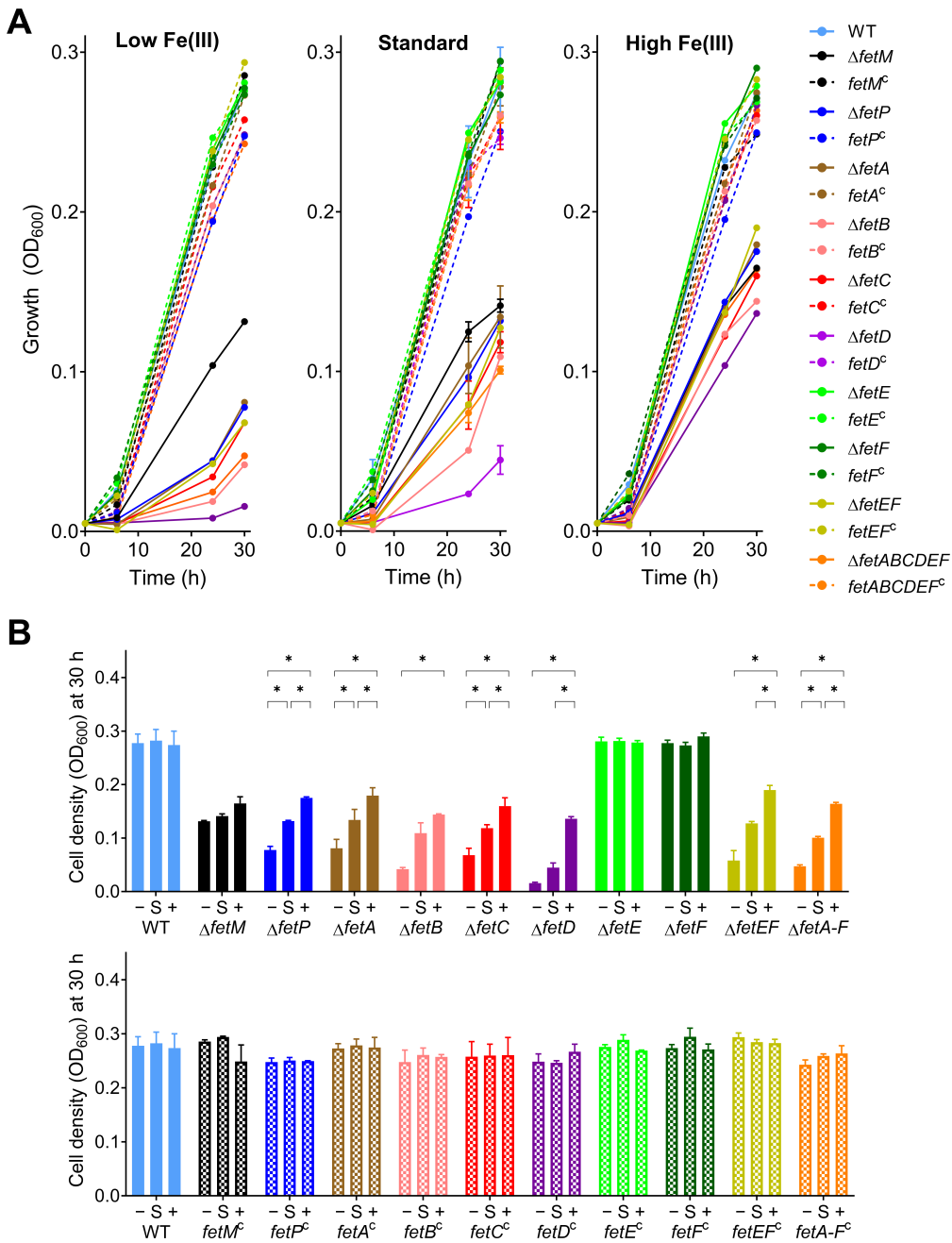


FIG 2 (A) Growth by monitoring OD₆₀₀ for *C. jejuni* gene deletion and complemented strains under different levels of iron availability. *C. jejuni* strains were cultured under depleted (–, MH with 5 μ M DFO), standard (S, MH), or high (+, MH supplemented with 100 μ M FeCl₃) iron availability. Each strain was assayed in triplicate except for WT, which was cultured for every growth experiment and hence was assayed with 18 biological replicates. Mean values are plotted with error bars representing standard deviation. (B) Cell density at the 30-h time point. Growth differences upon changing iron availability were compared for each strain with applied multi-strain comparison correction through two-stage step-up unpaired *t* tests (Benjamini, Krieger, and Yekutieli with 1% desired false discovery rate): **P* < 0.001.

$\Delta fetEF$ demonstrated intermediate growth, between that of wildtype and $\Delta fetABCDEF$ (Fig. S2B). At 8 and 16 μ g/mL of streptomycin, all strains showed minimal growth. Wild-type biphasic phenotypes and MICs were restored in all complemented strains (Fig. S2C and D).

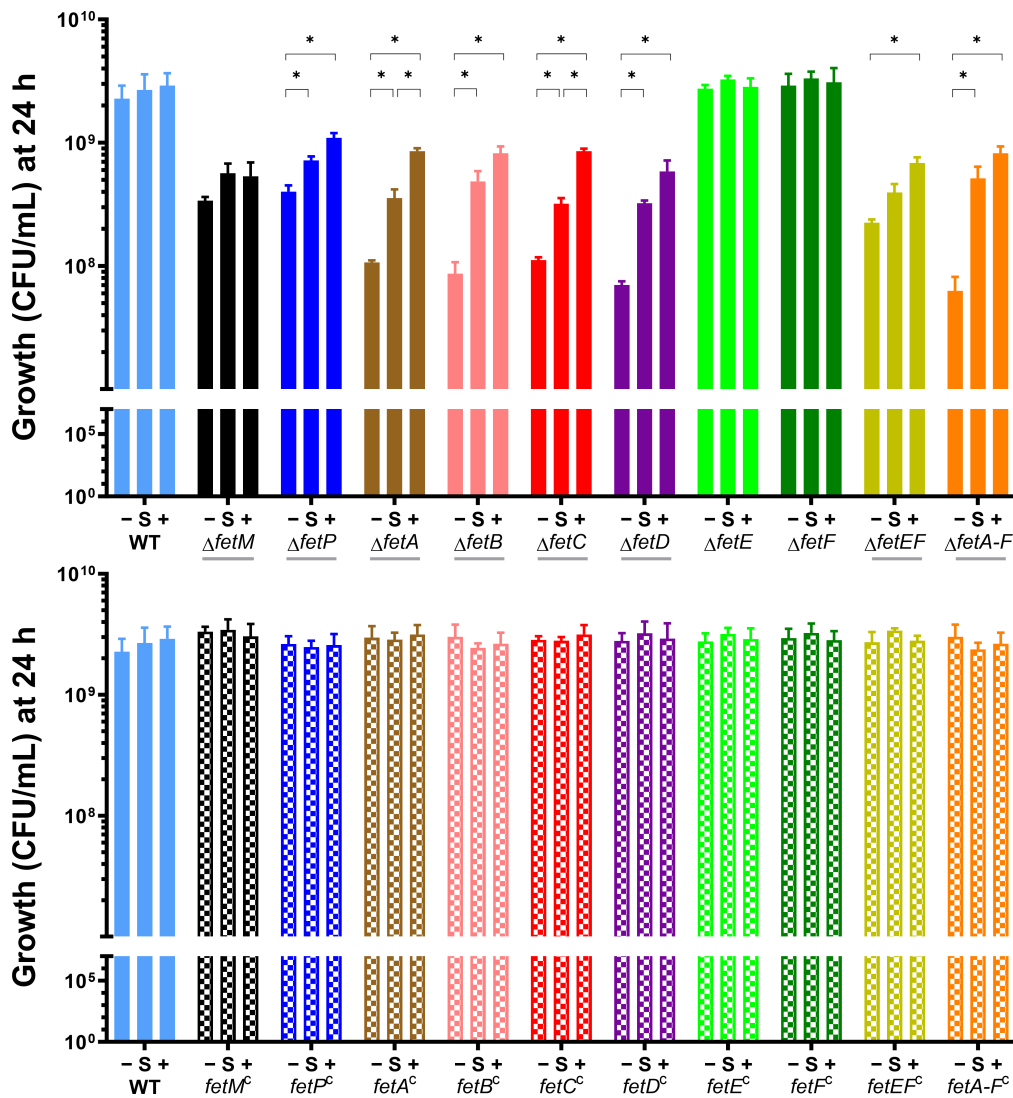


FIG 3 Growth of *C. jejuni* gene deletion and complemented strains over 24 h under different levels of iron availability, as monitored by CFU. *C. jejuni* strains were cultured under depleted (–, MH with 5 μM DFO), standard (S, MH), or high (+, MH supplemented with 100 μM FeCl₃) iron availability. Each strain was assayed in triplicate except for WT, which was cultured for every growth experiment and hence was assayed with 18 biological replicates. CFU/mL was determined for each culture by dilution plating (five technical replicates). Mean values are plotted with error bars representing standard deviation. Statistical comparison for each deletion mutant versus wildtype was first performed using unpaired *t*-tests: gray underlined strains indicate significance after Bonferroni correction with *P* < 0.005. Growth differences upon changing iron availability were then compared for each strain with applied multi-strain comparison correction through two-stage step-up unpaired *t*-tests (Benjamini, Krieger, and Yekutieli with 1% desired false discovery rate): **P* < 0.001.

Expression of *C. jejuni* FetA protein is independent of FetBCDEF

Due to the strong iron-dependent growth defect observed upon *fetA* deletion and the high level of *fetA* conservation in homologs of the *fet* gene cluster, *fetA* was selected as a gene to characterize further. To examine the protein expression levels of FetA under standard vs iron-limited conditions, a 2×Flag-tagged version of FetA was expressed in the Δ *fetA* and Δ *fetABCDEF* deletion strains using the pRRC-based *fetA* complementation vector (pRRC_1651; Fig. S1K) under the control of the chloramphenicol resistance cassette promoter. FetA^{2×Flag} was able to restore the growth of Δ *fetA*, indicating that the tag had not disrupted function (Fig. S3A). FetA^{2×Flag} was unable to restore the growth of Δ *fetABCDEF*, which expectedly mimicked the growth defect phenotypes of the individual

fetB to *fetD* deletion and *fetEF* double deletion strains. These strains were then analyzed by western blot, probing for FetA with a monoclonal anti-Flag tag antibody (Coomassie-stained SDS-PAGE loading control: Fig. S3B; western blot: Fig. S3C). No FetA band was observed in the $\Delta fetA$ and $\Delta fetABCDE$ controls. A band was observed for FetA in all tag-complemented strains, with higher protein levels under iron limitation. Full-length FetA is predicted to be ~54 kDa but ran slightly smaller than expected by SDS-PAGE and produced a smeared band when visualized by western blotting, likely due to the large transmembrane region of this protein.

C. jejuni FetE has capacity as a disulfide reductase

In light of our discovery that *fetE* and *fetF* function redundantly under iron limitation, along with the prediction that these genes encode thioredoxins, FetE was selected for further characterization by functional assays and structural analysis. *C. jejuni* FetE was recombinantly expressed in *E. coli* BL21(DE3) and purified. Far-western blot analysis (12) was used to screen for interactions between FetE, FetM, and FetP. While the expected interactions between FetM and FetP were observed, consistent with our previous work (12), no interactions of either FetM or FetP with FetE were detected (data not shown).

To verify whether *C. jejuni* FetE was capable of reducing disulfide bonds, an insulin disulfide reduction assay was selected as a standard method of thioredoxin characterization (26). The alpha and beta chains of insulin are linked by two disulfide bonds that can be reduced to precipitate the free beta chain. This produces an increase in absorbance at 650 nm that correlates to the rate of disulfide reduction, where baseline insulin reduction by dithiothreitol (DTT) can be increased by the addition of proteins with disulfide reductase activity. This assay was performed for *C. jejuni* FetE with comparison to a standard thioredoxin, *E. coli* Trx, and a blank sample (no protein added) representing baseline insulin reduction (Fig. 4).

The addition of *E. coli* Trx (6 μ M) drastically increased the rate of insulin reduction well above the disulfide reductase activity of baseline (no protein), with the rate observed here for *E. coli* Trx being similar to those observed in previous studies (26). The addition of *C. jejuni* FetE (60 μ M) also increased disulfide reduction above baseline, albeit to a lesser extent than *E. coli* Trx. Hence, these results indicate a capacity of *C. jejuni* FetE to mediate disulfide reduction.

C. jejuni FetE is structurally related to thioredoxins

The crystal structure of a soluble construct of FetE lacking the lipobox was solved as a monomer to 1.50 Å resolution. FetE consisted of a five-stranded β -sheet with three α -helices on one side and one short α -helix on the other. A structural similarity search

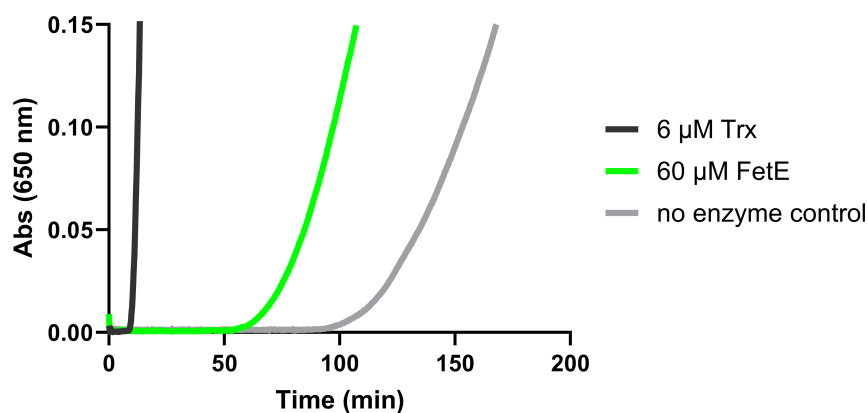


FIG 4 *C. jejuni* FetE exhibits disulfide reductase activity. Reduction of an intermolecular disulfide bond in bovine insulin (0.13 mM prepared in 0.1 M potassium phosphate pH 7.0, 2 mM EDTA, and 0.33 mM DTT) was monitored by an increase in absorbance at 650 nm.

of FetE against representative protein folds (PDB25) using the DALI server (27) revealed highest similarity to characterized proteins such as *Streptococcus gordonii* thiol-disulfide oxidoreductase SdbA (the top hit with Z-score 17.6; r.m.s.d. 2.1 Å over 133 Ca atoms; PDB ID: 5UM7) and *Mycobacterium tuberculosis* DsbE (Z-score 15.5; r.m.s.d. 2.2 Å over 127 Ca atoms; PDB ID: 1LU4). SdbA is an oxidase involved in the formation of disulfide-bonded proteins (28). Similarly, Mtb DsbE functions as an oxidase, which is atypical compared to the reductase role of its Gram-negative DsbE counterparts (29). Other top DALI hits remain uncharacterized. Alignment of 30 unique FetE homolog sequences (*E*-value cutoff = 0.0001) mapped onto the surface of the FetE crystal structure using Consurf (30) revealed conservation of the predicted key catalytic CXXC motif, which are the most highly conserved residues on the surface of FetE (Fig. S4).

Deletion of *fetEF* affects DTNB reduction by *C. jejuni* cell-free extracts

As predicted thioredoxins, FetE and FetF are hypothesized to mediate disulfide homeostasis in *C. jejuni*. To probe for differences in disulfide reduction capacity, extracts of *C. jejuni* wildtype, $\Delta fetE$, $\Delta fetF$, and $\Delta fetEF$ were assayed with the colorimetric agent 5,5'-dithiobis-(2-nitrobenzoic acid) (DTNB). DTNB consists of two aromatic groups linked by a disulfide bond, with disulfide reduction resulting in the production of a thiol anion that absorbs strongly at 412 nm. Cell-free extracts were prepared from *C. jejuni* wildtype, $\Delta fetE$, $\Delta fetF$, and $\Delta fetEF$, normalized for total protein concentration, and then incubated with DTNB and NADH in a cuvette for spectrophotometric determination of the disulfide reduction rate (Fig. 5).

Similar DTNB reduction rates were observed for cell extracts from *C. jejuni* wildtype (0.0110 ± 0.0014 Abs_{412nm}/min), $\Delta fetE$ (0.0105 ± 0.0009 Abs_{412nm}/min), and $\Delta fetF$ (0.0135 ± 0.0042 Abs_{412nm}/min) strains. Comparatively, *C. jejuni* $\Delta fetEF$ cell extract showed a significantly higher rate of DTNB reduction (0.0359 ± 0.0042 Abs_{412nm}/min).

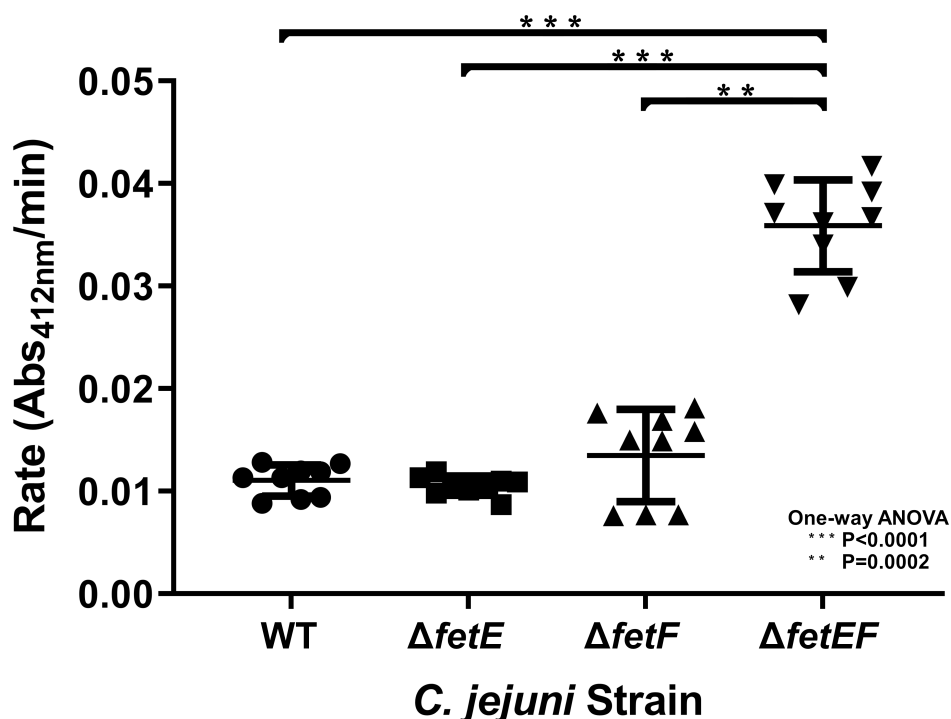


FIG 5 DTNB reduction by *C. jejuni* wildtype, $\Delta fetE$, $\Delta fetF$, and $\Delta fetEF$ cell extracts. The overall rate for each strain represents extracts from three mid-log phase cultures incubated for 3 h under iron limitation (5 μ M DFO). Reduction of 0.1 mM DTNB in 0.2 mM NADPH and 50 mM Tris-HCl pH 7.2 by each extract was performed three times, with means and error bars representing standard deviation and statistical significance determined by one-way ANOVA.

DISCUSSION

In addressing the extensive global morbidity and socioeconomic burden caused by *C. jejuni*, it is of high priority to gain a deeper understanding of the molecular systems that support virulence during infection, such as the upregulated *fetMP-fetABCDEF* gene cluster. In this study, we systematically deconstructed the *fetMP-fetABCDEF* gene cluster to assess the role of each gene in *C. jejuni* growth during iron scarcity as well as the functionality of one of the predicted oxidoreductase proteins.

Other than the individual thioredoxin deletion strains $\Delta fetE$ and $\Delta fetF$, every tested deletion strain exhibited growth defects. However, no strain was completely devoid of growth, suggesting that other iron uptake systems in *C. jejuni* are responsible for the partial growth observed upon the deletion of *fet* genes. Unexpectedly, the deletion of *fetM* resulted in a growth defect not significantly correlated with iron availability, whereas all other deletion strains with growth defects exhibited greater growth restoration upon increased iron availability. For the Fet cluster, only homologs of FetM have, to date, been shown to directly transport iron (17, 18). Together, this suggests that the other iron-uptake systems are unable to fully compensate for $\Delta fetM$ growth under ferric chloride supplementation, supporting the key role of FetM in direct iron transport.

The other *fet* genes, with a proposed role in supporting iron transport through FetM, exhibited growth patterns with a stronger dependency on iron availability. Full growth restoration was not observed upon iron supplementation, possibly due to the low solubility (and hence lower bioavailability) of ferric chloride. However, the high sensitivity observed for $\Delta fetA$, $\Delta fetB$, $\Delta fetC$, and $\Delta fetD$ to iron levels was comparable to that of $\Delta fetP$, which directly supports FetM function (12), highlighting an equally important role for the individual FetA and FetBCD proteins under iron limitation. This is reinforced by the high conservation of equivalent genes in all known homologs of the *fetMP-fetABCDEF* cluster across several bacterial phyla (10).

The biochemical function of FetA is not known, but it likely reflects the presence of two predicted periplasmic domains (DUF2318 and YHS). Similar to the thioredoxins FetE and FetF, the DUF2318 domain contains conserved Cys residues. Four of the five Cys residues in DUF2318 constitute two CXXC motifs (CMIC and CISC) that may have a redox role through disulfide formation. The observation of higher FetA protein levels under iron limitation across all 2×Flag-tag-complemented strains suggests that FetA expression may be iron-modulated. The FetA^{2×Flag} construct included the intergenic region between *fetP* and *fetA*, with *fetA* expression under the control of a constitutively expressing Cm promoter. As the Cm promoter is not iron-regulated (31), this suggests the presence of regulatory elements either in the intergenic region between *fetP* and *fetA* present in the complementation construct or within *fetA* itself. Alternatively, *fetA* may be post-transcriptionally regulated. The growth of $\Delta fetA^{2\times\text{Flag-fetA}}$ was comparable to $\Delta fetA^c$ and wild-type strains, demonstrating that tagged FetA is functional. Therefore, the detection of 2×Flag-FetA in both $\Delta fetA^{2\times\text{Flag-fetA}}$ and $\Delta fetABCDEF^{2\times\text{Flag-fetA}}$ suggests that FetA is stably expressed in the presence and absence of FetBCDEF.

If FetMP-FetABCDEF represents one iron uptake system in which FetM is the sole iron permease, then the function (and substrate) for the putative ABC transporter encoded by *fetBCD* remains unclear. ABC transporters are a common component of bacterial iron uptake systems, with ATP hydrolysis often driving the passage of a Fe-siderophore complex from the periplasm to the cytoplasm through a channel formed by the two transmembrane proteins (32). Despite homology between *fetB* and *fetC* (28% sequence identity), deletion of either gene resulted in a strong growth defect, indicating that both genes are required for transporter function. This suggests the specific requirement of a FetB-FetC heterodimer for the proper function of this gene cluster and that FetB-FetB or FetC-FetC homodimers are either not formed or cannot sufficiently restore the growth defects of $\Delta fetB$ or $\Delta fetC$.

Individual deletion of *fetE* or *fetF* in *C. jejuni* did not correspond to a growth defect under any level of iron availability, whereas the deletion of both genes ($\Delta fetEF$) resulted in a growth defect in the iron-restricted medium. This suggests that *fetE* and *fetF* perform

redundant functions to support *C. jejuni* growth during iron restriction, as the presence of either gene is sufficient to maintain growth comparable to wildtype. All *fet* deletion strains exhibited increased sensitivity to streptomycin, suggesting that iron homeostasis is important in antibiotic resistance. However, the streptomycin sensitivity of $\Delta fetE$, $\Delta fetF$, and $\Delta fetEF$ were intermediate compared to the other deletion strains. The *fetE* and *fetF* genes are homologs (22% amino acid sequence identity) predicted to encode periplasmic, membrane-associated protein disulfide reductases. We demonstrated that FetE contains a thioredoxin fold and can reduce insulin disulfide. However, the comparatively slow rate of insulin reduction by FetE compared to *E. coli* Trx, the structural similarity to the thiol-disulfide oxidases SdbA and DsbE, and the higher rate of DTNB reduction by extracts of *C. jejuni* $\Delta fetEF$ than those of wildtype, $\Delta fetE$, and $\Delta fetF$ suggest that the primary role of FetE and FetF may be to act as oxidases *in vivo*. This would be consistent with our previous observation that *C. jejuni* $\Delta fetABCDE$ had greater survival than wildtype upon exposure to oxidative stress (10), which suggested that the presence of FetABCDE increased susceptibility to the deleterious effects of oxidation.

Overall, the experimental results described here have advanced understanding on the collective roles of the Fet system components in relation to *C. jejuni* growth under iron limitation. In combining these new findings with an *in silico* investigation and prior literature, we propose an updated model for how the system encoded by *fetMP-fetABCDE* may function (Fig. 6). In this revised model, an iron-chelator complex first passes through the outer membrane via an as yet unidentified transporter. Upon entering the periplasm, the iron is released from the chelator and transported into the cytoplasm by the cooperative action of the iron-binding protein FetP and the iron permease FetM. Our previous studies in *C. jejuni* and uropathogenic *E. coli* strongly suggest an iron oxidation/reduction-based mechanism for iron transport (11, 12, 18). Based on our studies presented here, we predict that FetE and FetF play overlapping roles in supporting FetMP-based iron transport by actively relaying the necessary reducing power likely sourced from FetB, FetC, and FetD, functioning as a single heteromeric ABC transporter, and through FetA. In the absence of FetM, a major route for iron to cross the inner membrane, growth is impaired irrespective of the presence of other Fet proteins, making this strain more resistant to growth recovery upon iron supplementation. FetA, FetBCD, and FetEF, conversely, each critically support the redox dependency of the FetMP iron uptake function. Hence, the deletion of components from FetABCDE results in the growth of FetMP-intact strains that are more dependent on overall iron availability. Despite being a double-edged sword, as FetABCDE increases susceptibility to oxidative stress (10), we demonstrate that this cluster is conserved because it plays an important role in cell growth in conjunction with FetMP.

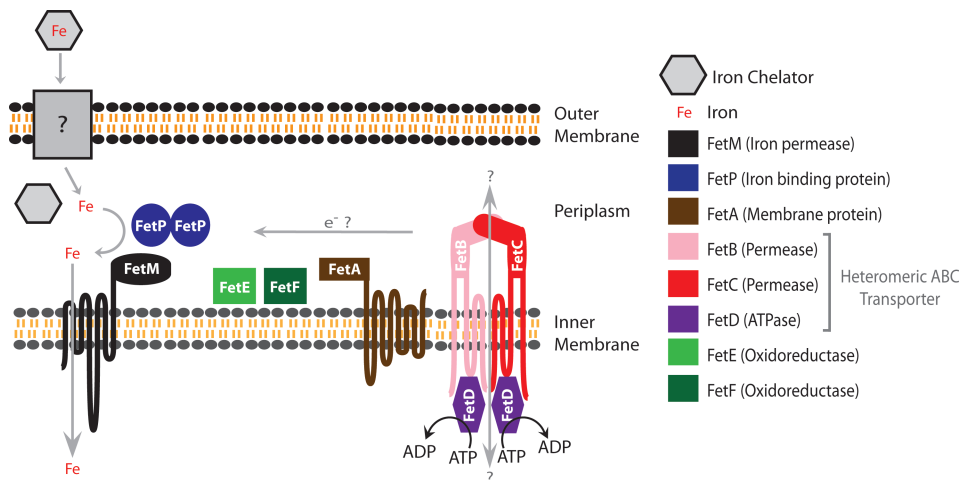


FIG 6 Model of the FetMP-FetABCDE system based on predicted and known functions in iron transport. Adapted and updated from Liu et al. (10).

Conclusion

The significant global disease burden caused by *C. jejuni* has provided an impetus for research into novel systems important for pathogenesis and pathogenesis-related attributes. The *fetMP-fetABCDEF* genes have stood out as highly upregulated during human infection and in the presence of human fecal extracts, with only recent work bringing the importance of the downstream cluster *fetABCDEF* to light. This study has addressed gaps in knowledge relating to the *C. jejuni fetMP-fetABCDEF* gene cluster through a combined microbial genetics, molecular biology, biochemistry, and structural biology approach. All components of this gene cluster emerged as determinants of growth during iron scarcity, a known virulence-determining factor during *C. jejuni* infection. Expression of the integral membrane protein FetA was shown to be independent of FetBCDEF. FetBCD likely forms a heteromeric ABC transporter essential to the function of the Fet cluster. *C. jejuni* FetE most closely resembles the structure of thiol-disulfide oxidases and demonstrated comparatively poorer disulfide reduction activity. Additionally, cell extracts from the deletion of *fetEF* exhibited the greatest reduction activity, together suggesting that FetE and FetF may function as oxidases *in vivo*.

MATERIALS AND METHODS

Design and construction of *C. jejuni* gene deletion and complemented strains

For gene deletion strains, the wild-type gene along with flanking regions was cloned into a pGEM-T plasmid with 45%–90% of the gene replaced with a non-polar *aphA3* kanamycin (Km)-resistance cassette (Table S1). Natural transformation of the modified pGEM suicide vector into *C. jejuni* allowed the replacement of the target gene by homologous recombination at the flanking regions (Fig. S1A through I). For complemented strains, the wild-type gene was cloned into pRRC, which was naturally transformed into its respective *C. jejuni* mutant strain for integration of the gene and an upstream chloramphenicol (Cm)-resistance cassette at one or more of three ectopic loci in the chromosome (33) (Fig. S1J and K).

A list of all strains, plasmids, and primers used during construction for each strain is provided in Table S1. *C. jejuni* 81–176 (clinical isolate from diarrheic patient) was used as the wild-type strain for all experiments (34). Plasmids and strains were verified by PCR analysis followed by Sanger sequencing (Genewiz). The growth conditions for *C. jejuni* and *E. coli*, detailed strain construction protocols, and determination of total iron content in the standard medium by ICP-MS are described in the Supplemental Methods.

C. jejuni growth experiments for sensitivity to iron availability

All *C. jejuni* strains were grown overnight on MH-TV agar plates with Km (deletion strains) or Cm (complemented strains), streaked onto fresh equivalent plates, and then grown for another 6 h. Cells were harvested and resuspended in MH-TV broth (10 mL) to an OD₆₀₀ of 0.0004 (WT), 0.002 (all complemented strains), 0.005 ($\Delta fetE$, $\Delta fetF$), or 0.02 (all other deletion mutants) to consistently achieve cells in the mid-log-phase (OD₆₀₀ of 0.3–0.6) after a further 18 h of shaking incubation (200 rpm). Mid-log-phase cultures were resuspended in fresh 2× MH-TV and then dispensed into 96 well plates containing equivalent volume aqueous solutions of DFO (10 μ M), water, or FeCl₃ (200 μ M) to achieve 200 μ L 1× MH-TV starting cultures at an initial OD₆₀₀ of 0.005, corresponding to low iron (MH-TV + 5 μ M DFO), standard (MH-TV), and high iron (MH-TV + 100 μ M FeCl₃) conditions. Throughout incubation, growth was monitored by OD₆₀₀ (Thermo Fisher Scientific Varioskan Flash plate reader) at 0, 6, 24, and 30 h, and by CFUs at 0 and 24 h. CFU/mL values calculated for each culture at 24 h were divided by the CFU/mL at 0 h to represent the amount of growth in each culture (CFU_{24/0}). All strains were assessed with three biological replicates for each level of iron availability, and CFUs were determined using five technical replicates. Statistical differences were calculated using the Student's *t*-test.

***C. jejuni* growth experiments for sensitivity to streptomycin**

Full experimental details are described in the Supplemental Methods.

Expression of 2×Flag-tagged FetA in *C. jejuni*

A C-terminal 2× repeat Flag-tag was inserted into *C. jejuni* *fetA* by FastCloning (35) using the constitutively expressing complementation vector pRRC_1651 as a template (Fig. S1K) and Q5 DNA polymerase. pRRC_1651 includes 93 C-terminal bp of *fetP*, 82 bp of the intergenic region, and the complete 1,404 bp of the *fetA* gene. *C. jejuni* strains Δ *fetA* and Δ *fetABCDE*F were then complemented with this construct following the method to generate Δ *fetA*^c, producing Δ *fetA*^{2×Flag-FetA} and Δ *fetABCDE*F^{2×Flag-FetA}. Successful insertion was confirmed by sequencing purified genomic DNA. Methods to confirm the proper functionality of the tagged FetA variant in the deletion strains are described in the Supplemental Methods.

To examine the expression of tagged FetA in *C. jejuni*, the variant-complemented strains were grown to mid-log-phase in 15 mL MH-TV, resuspended in fresh MH-TV supplemented with or without 10 μ M DFO, and pelleted after 3 h of growth. The harvested cell pellets were analyzed by SDS-PAGE and probed by western blot with an anti-Flag antibody (Genscript A01868).

Expression of *C. jejuni* FetE and other Fet proteins

The expression vector for *C. jejuni* FetE was synthesized by GeneArt (Invitrogen) into pET151/D-TOPO. The DNA sequence encoded an N-terminal 6×His tag, a V5 epitope, a TEV cut site, and residues IDPFT followed by amino acids 22–162 of native FetE (CJ81176_1655). This vector was transformed into *E. coli* BL21(DE3) for expression and purification, following the protocol for *E. coli* FetA with slight modifications. Cells were induced with 0.25 mM IPTG, lysed in 30 mM Tris, 200 mM NaCl, 5 mM imidazole, and 2 mM TCEP, pH 7.5 and dialyzed into 30 mM Tris, 100 mM NaCl, and 2 mM TCEP, pH 7.5 after His-tag removal with TEV protease. TEV protease was removed with a second nickel resin purification step using dialysis buffer and concentrated. *C. jejuni* FetM and FetP were prepared as part of other studies (11, 12).

FetE crystallization and structure determination

FetE was crystallized in space group P2₁ under 1.8 M ammonium sulfate and 0.1 M sodium acetate. Crystals were then soaked in 0.06 M sodium acetate, 1.6 M ammonium sulfate, and 0.5 M sodium iodide, cryoprotected using 30% glycerol, flash frozen with liquid nitrogen, and sent to the SSRL beamline 9-2. A 1.95-Å resolution data set was collected at 1.6 Å wavelength, and iodide phasing was used to successfully solve the crystal structure. This structure was then used for molecular replacement against a non-iodide-soaked 1.5-Å resolution data set collected at CLS beamline CMCF-ID. Data collection and refinement statistics are summarized in Table S2.

***C. jejuni* cell extracts and DTNB reduction assay**

Protocols for the colorimetric DTNB reduction assay with *C. jejuni* cell extracts were adapted from the methods used by Kaakoush et al. (36) to identify *C. jejuni* protein disulfide reductases (36). *C. jejuni* cell extract preparation and the adapted assay are described in the Supplemental Methods.

ACKNOWLEDGMENTS

The authors acknowledge the significant contributions and mentorship of the late Professor Erin C. Gaynor to this work, and we are grateful for Dr. Gaynor's family's support in seeing this work published. We also thank Martha Liu for providing constructive input to the project and Jina Yeom for her preliminary work on the streptomycin sensitivity

assays. We thank Jenny Wallace and Emilisa Frirdich for training in designing deletion and complementation strains, as well as training for *C. jejuni* growth assays.

This research was supported by grants from the Michael Smith Foundation for Health Research (MSFHR) to T.R.-S. (RT 18437), Canadian Institutes of Health Research (CIHR) to E.C.G. (MOP-68981), and a Natural Science and Engineering (NSERC) Discovery Grant to M.E.P.M. (RGPIN-2022-04568). Use of the Stanford Synchrotron Radiation Lightsource, SLAC National Accelerator Laboratory, is supported by the U.S. Department of Energy, Office of Science, Office of Basic Energy Sciences under Contract No. DE-AC02-76SF00515. The SSRL Structural Molecular Biology Program is supported by the DOE Office of Biological and Environmental Research and by the National Institutes of Health, National Institute of General Medical Sciences (P30GM133894). The contents of this publication are solely the responsibility of the authors and do not necessarily represent the official views of NIGMS or NIH. Part of the research described in this paper was also performed using beamline CMCF-ID at the Canadian Light Source, a national research facility of the University of Saskatchewan, which is supported by the Canada Foundation for Innovation (CFI), the Natural Sciences and Engineering Research Council (NSERC), the National Research Council (NRC), the Canadian Institutes of Health Research (CIHR), the Government of Saskatchewan, and the University of Saskatchewan.

AUTHOR AFFILIATION

¹Department of Microbiology and Immunology, The University of British Columbia, Vancouver, British Columbia, Canada

PRESENT ADDRESS

Tomas Richardson-Sanchez, IQVIA, Sydney, NSW, Australia

AUTHOR ORCIDs

Tomas Richardson-Sanchez  <http://orcid.org/0000-0002-8925-9064>

Anson C. K. Chan  <http://orcid.org/0000-0001-6625-8942>

Erin C. Gaynor  <http://orcid.org/0000-0001-5847-7205>

Michael E. P. Murphy  <http://orcid.org/0000-0003-2589-0014>

FUNDING

Funder	Grant(s)	Author(s)
Michael Smith Health Research BC (MSFHR)	RT 18437	Tomas Richardson-Sanchez
Gouvernement du Canada Canadian Institutes of Health Research (IRSC)	MOP-68981	Erin C. Gaynor
Gouvernement du Canada Natural Sciences and Engineering Research Council of Canada (NSERC)	RGPIN-2022-04568	Michael E. P. Murphy

DATA AVAILABILITY

The coordinates and observed structure factor amplitudes have been deposited in the PDB under the accession code [8T4C](#).

ADDITIONAL FILES

The following material is available [online](#).

Supplemental Material

Supplemental material (Spectrum03148-23-s0001.pdf). Supplemental methods, Fig. S1 to S4, and Tables S1 and S2.

REFERENCES

1. Whiley H, van den Akker B, Giglio S, Bentham R. 2013. The role of environmental reservoirs in human campylobacteriosis. *Int J Environ Res Public Health* 10:5886–5907. <https://doi.org/10.3390/ijerph10115886>
2. Wilson DJ, Gabriel E, Leatherbarrow AJH, Cheesbrough J, Gee S, Bolton E, Fox A, Fearnhead P, Hart CA, Diggle PJ. 2008. Tracing the source of campylobacteriosis. *PLoS Genet* 4:e1000203. <https://doi.org/10.1371/journal.pgen.1000203>
3. Blaser MJ. 1997. Epidemiologic and clinical features of *Campylobacter jejuni* infections. *J Infect Dis* 176:S103–S105. <https://doi.org/10.1086/513780>
4. Keithlin J, Sargeant J, Thomas MK, Fazil A. 2014. Systematic review and meta-analysis of the proportion of *Campylobacter* cases that develop chronic sequelae. *BMC Public Health* 14:1203. <https://doi.org/10.1186/1471-2458-14-1203>
5. Walker RI, Caldwell MB, Lee EC, Guerry P, Trust TJ, Ruiz-Palacios GM. 1986. Pathophysiology of *Campylobacter* enteritis. *Microbiol Rev* 50:81–94. <https://doi.org/10.1128/mr.50.1.81-94.1986>
6. García-Fernández A, Dionisi AM, Arena S, Iglesias-Torrens Y, Carattoli A, Luzzi I. 2018. Human campylobacteriosis in Italy: emergence of multi-drug resistance to ciprofloxacin, tetracycline, and erythromycin. *Front Microbiol* 9:1906. <https://doi.org/10.3389/fmicb.2018.01906>
7. Kayman T, Abay S, Aydin F, Şahin O. 2019. Antibiotic resistance of *Campylobacter jejuni* isolates recovered from humans with diarrhoea in Turkey. *J Med Microbiol* 68:136–142. <https://doi.org/10.1099/jmm.0.000890>
8. Woźniak-Biel A, Bugla-Płoskońska G, Kielsznia A, Korzekwa K, Tobiasz A, Korzeniowska-Kowal A, Wieliczko A. 2018. High prevalence of resistance to fluoroquinolones and tetracycline *Campylobacter* spp. isolated from poultry in Poland. *Microb Drug Resist* 24:314–322. <https://doi.org/10.1089/mdr.2016.0249>
9. Crofts AA, Poly FM, Ewing CP, Kuroiwa JM, Rimmer JE, Harro C, Sack D, Talaat KR, Porter CK, Gutierrez RL, DeNearing B, Brubaker J, Laird RM, Maue AC, Jaep K, Alcalá A, Tribble DR, Riddle MS, Ramakrishnan A, McCoy AJ, Davies BW, Guerry P, Trent MS. 2018. *Campylobacter jejuni* transcriptional and genetic adaptation during human infection. *Nat Microbiol* 3:494–502. <https://doi.org/10.1038/s41564-018-0133-7>
10. Liu MM, Boinett CJ, Chan ACK, Parkhill J, Murphy MEP, Gaynor EC. 2018. Investigating the *Campylobacter jejuni* transcriptional response to host intestinal extracts reveals the involvement of a widely conserved iron uptake system. *mBio* 9:e01347-18. <https://doi.org/10.1128/mBio.01347-18>
11. Chan ACK, Doukov TI, Scofield M, Tom-Yew SAL, Ramin AB, Mackichan JK, Gaynor EC, Murphy MEP. 2010. Structure and function of P19, a high-affinity iron transporter of the human pathogen *Campylobacter jejuni*. *J Mol Biol* 401:590–604. <https://doi.org/10.1016/j.jmb.2010.06.038>
12. Chan ACK, Lin H, Koch D, Grass G, Nies DH, Murphy MEP. 2020. A copper site is required for iron transport by the periplasmic proteins P19 and FetP. *Metallomics* 12:1530–1541. <https://doi.org/10.1039/d0mt00130a>
13. Butcher J, Handley RA, van Vliet AHM, Stintzi A. 2015. Refined analysis of the *Campylobacter jejuni* iron-dependent/independent Fur- and PerR-transcriptomes. *BMC Genomics* 16:498. <https://doi.org/10.1186/s12864-015-1661-7>
14. Holmes K, Mulholland F, Pearson BM, Pin C, McNicholl-Kennedy J, Ketley JM, Wells JM. 2005. *Campylobacter jejuni* gene expression in response to iron limitation and the role of Fur. *Microbiology (Reading)* 151:243–257. <https://doi.org/10.1099/mic.0.27412-0>
15. Palyada K, Threadgill D, Stintzi A. 2004. Iron acquisition and regulation in *Campylobacter jejuni*. *J Bacteriol* 186:4714–4729. <https://doi.org/10.1128/JB.186.14.4714-4729.2004>
16. Dugar G, Herbig A, Förstner KU, Heidrich N, Reinhardt R, Nieselt K, Sharma CM. 2013. High-resolution transcriptome maps reveal strain-specific regulatory features of multiple *Campylobacter jejuni* isolates. *PLoS Genet* 9:e1003495. <https://doi.org/10.1371/journal.pgen.1003495>
17. Grosse C, Scherer J, Koch D, Otto M, Taudte N, Grass G. 2006. A new ferrous iron-uptake transporter, EfeU (YcdN), from *Escherichia coli*. *Mol Microbiol* 62:120–131. <https://doi.org/10.1111/j.1365-2958.2006.05326.x>
18. Koch D, Chan ACK, Murphy MEP, Lillie H, Grass G, Nies DH. 2011. Characterization of a dipartite iron uptake system from uropathogenic *Escherichia coli* strain F11. *J Biol Chem* 286:25317–25330. <https://doi.org/10.1074/jbc.M111.222745>
19. Brickman TJ, Armstrong SK. 2012. Iron and pH-responsive FtrABCD ferrous iron utilization system of *Bordetella* species. *Mol Microbiol* 86:580–593. <https://doi.org/10.1111/mmi.12003>
20. Fetherston JD, Mier I, Truszczynska H, Perry RD. 2012. The Yfe and Feo transporters are involved in microaerobic growth and virulence of *Yersinia pestis* in bubonic plague. *Infect Immun* 80:3880–3891. <https://doi.org/10.1128/IAI.00086-12>
21. Stintzi A, van Vliet AH, Ketley JM. 2008. Iron metabolism, transport, and regulation, p 591–610. In Nachamkin I, CM Szymanski, MJ Blaser (ed), *Campylobacter*, 3rd ed. ASM Press, Washington, DC.
22. Baig BH, Wachsmuth IK, Morris GK. 1986. Utilization of exogenous siderophores by *Campylobacter* species. *J Clin Microbiol* 23:431–433. <https://doi.org/10.1128/jcm.23.3.431-433.1986>
23. Field LH, Headley VL, Payne SM, Berry LJ. 1986. Influence of iron on growth, morphology, outer membrane protein composition, and synthesis of siderophores in *Campylobacter jejuni*. *Infect Immun* 54:126–132. <https://doi.org/10.1128/iai.54.1.126-132.1986>
24. Zeller T, Klug G. 2006. Thioredoxins in bacteria: functions in oxidative stress response and regulation of thioredoxin genes. *Naturwissenschaften* 93:259–266. <https://doi.org/10.1007/s00114-006-0106-1>
25. Girardello R, Bispo PJM, Yamanaka TM, Gales AC. 2012. Cation concentration variability of four distinct Mueller-Hinton agar brands influences polymyxin B susceptibility results. *J Clin Microbiol* 50:2414–2418. <https://doi.org/10.1128/JCM.06686-11>
26. Holmgren A. 1979. Thioredoxin catalyzes the reduction of insulin disulfides by dithiothreitol and dihydrolipoamide. *J Biol Chem* 254:9627–9632. [https://doi.org/10.1016/S0021-9258\(19\)83562-7](https://doi.org/10.1016/S0021-9258(19)83562-7)
27. Holm L. 2020. Using dali for protein structure comparison. *Methods Mol Biol* 2112:29–42. https://doi.org/10.1007/978-1-0716-0270-6_3
28. Davey L, Ng CKW, Halperin SA, Lee SF. 2013. Functional analysis of paralogous thiol-disulfide oxidoreductases in *Streptococcus gordonii*. *J Biol Chem* 288:16416–16429. <https://doi.org/10.1074/jbc.M113.464578>
29. Goulding CW, Apostol MI, Gleiter S, Parseghian A, Bardwell J, Gennaro M, Eisenberg D. 2004. Gram-positive DsbE proteins function differently from Gram-negative DsbE homologs. A structure to function analysis of DsbE from *Mycobacterium tuberculosis*. *J Biol Chem* 279:3516–3524. <https://doi.org/10.1074/jbc.M311833200>
30. Ashkenazy H, Abadi S, Martz E, Chay O, Mayrose I, Pupko T, Ben-Tal N. 2016. ConSurf 2016: an improved methodology to estimate and visualize evolutionary conservation in macromolecules. *Nucleic Acids Res* 44:W344–W350. <https://doi.org/10.1093/nar/gkw408>
31. Wooldridge KG, Williams PH, Ketley JM. 1994. Iron-responsive genetic regulation in *Campylobacter jejuni*: cloning and characterization of a fur homolog. *J Bacteriol* 176:5852–5856. <https://doi.org/10.1128/jb.176.18.5852-5856.1994>
32. Krewulak KD, Vogel HJ. 2008. Structural biology of bacterial iron uptake. *Biochim Biophys Acta* 1778:1781–1804. <https://doi.org/10.1016/j.bbamem.2007.07.026>
33. Karlyshev AV, Wren BW. 2005. Development and application of an insertional system for gene delivery and expression in *Campylobacter jejuni*. *Appl Environ Microbiol* 71:4004–4013. <https://doi.org/10.1128/AEM.71.7.4004-4013.2005>
34. Korlath JA, Osterholm MT, Judy LA, Forfang JC, Robinson RA. 1985. A point-source outbreak of campylobacteriosis associated with consumption of raw milk. *J Infect Dis* 152:592–596. <https://doi.org/10.1093/infdis/152.3.592>

35. Li C, Wen A, Shen B, Lu J, Huang Y, Chang Y. 2011. FastCloning: a highly simplified, purification-free, sequence- and ligation-independent PCR cloning method. *BMC Biotechnol* 11:92. <https://doi.org/10.1186/1472-6750-11-92>
36. Kaakoush NO, Sterzenbach T, Miller WG, Suerbaum S, Mendz GL. 2007. Identification of disulfide reductases in Campylobacterales: a bioinformatics investigation. *Antonie Van Leeuwenhoek* 92:429–441. <https://doi.org/10.1007/s10482-007-9171-5>